# Evolution of induced patterns in surface-tension-driven Bénard convection

P. Cerisier
*Institut Universitaire des Systemes Thermiques Industriels, Université de Provence, 13397 Marseille CEDEX 13, France*

C. Perez-Garcia
*Departamento de Fisica, Faculdad de Ciencias, Universidad de Navarra, Pamplona, Spain and Departament de Fisica Fondamental, Universitat de Barcelona, Barcelona, Spain*

R. Occelli
*Institut Universitaire des Systemes Thermiques Industriels, Université de Provence, 13397 Marseille CEDEX 13, France*
(Received 30 November 1992)

Experimental results on the evolution of induced patterns in Bénard-Marangoni convection are reported. These patterns are initially forced by means of a thermal technique which allows the formation of a regular hexagonal pattern with a chosen wavelength. Several series of measurements have been performed in square vessels with different aspect ratios $\Gamma$. For fixed $\Gamma$, after inducing a pattern with a wavelength different from the optimal one, an evolution is observed that leads to an evolving mean wavelength. The main mechanism for this evolution is the generation of defects which increase the disorder in the pattern. This disorder is mainly due to nucleation of new cells when the forced ones are too large, or by fusion of cells when the original ones are too small. Another interesting phenomenon occurs when the forced wavelength $\lambda$ is close to the optimal one. In large-aspect-ratio vessels the disorder rises initially at the center of the pattern, leading to a relaxation of the mean wavelength. However, in small-aspect-ratio vessels, the behavior can be nonmonotonous. Under well-chosen conditions (the initial pattern has a mean wavelength slightly smaller than the optimal one), $\lambda$ increases initially as a consequence of sidewall effects; then it decreases due to the rising and propagation of a dislocation line in the pattern. This evolution has a form similar to the creep function in a viscoelastic material. This effect seems to provide an effective wavelength selection mechanism. Using a Ginzburg-Landau model adapted to the hexagonal lattice, the relative importance of local wavelength variations, disalignment of polygon lines, defects, and sidewalls have been determined.

PACS number(s): 47.20.−k, 44.25.+f

## I. INTRODUCTION

In recent years an increasing interest in structured patterns in systems out of equilibrium can be noticed. The Rayleigh-Bénard (RB) instability provides a prototype of systems of such patterns. Usually in this instability, the pattern is formed by rolls. The goal of many studies was to determine the wave-number selection mechanism and the contribution of different factors (lateral walls, relation between the depth and the horizontal extent of the layer, heating rate, etc.) on the final selected wave number [1]. Related to this problem is the evolution of defects in these patterns of rolls which, finally, can lead to a disordered motion beyond a critical heating. Another interesting problem, yet unsolved, is the relation between this spatial disorder and some chaotic motions.

In a surface-tension-driven instability (Bénard instability) convective motions develop in an almost regular hexagonal pattern with some defects always present. In recent works the influence of the parameters of the fluid and of the container on the generation and evolution of defects in spontaneous patterns has been studied [2].

Although patterns in Bénard convection were described for the first time in 1900 [3], systematic experimental works on hexagonal convective patterns arising in this case are not so numerous as in the RB case. This is due, in part, to the scarce and incomplete theoretical development [4] and partially, to the difficulties in controlling some boundary conditions, in particular the interaction between the liquid and the air in contact with it. From the theoretical point of view a systematic work, similar to that done by Busse [5] for RB instability, still lacks in Bénard convection.

One of the more useful techniques for analyzing the rich assortment of possible secondary instabilities acting on a pattern of rolls in RB convection is the shadowgraph technique developed by Chen and Whitehead [6]. It consists in placing a grid with a given wavelength and provoking an extra heating which forces the rolls to appear with this wave number. This provides a well-defined initial condition. In a series of articles Busse and Whitehead described the different secondary instabilities [7] in RB convection. Those new instabilities appear when the initial pattern has a wave number out of the roll stability region.

This technique cannot be adapted directly to produce hexagonal patterns in Bénard convection because the air layer between the grid and the liquid perturbs the local heating from the lamp. Instead of this, an alternative "thermal technique" has been proposed, allowing us to impose an initial pattern in a liquid with an upper free surface open to the atmosphere [8].

 

The aim of the present paper is to present some experimental results obtained using this technique. It is applied to force initial patterns in square vessels with different aspect ratios (the aspect ratio $\Gamma$ is a nondimensional number which accounts for the box size; it is defined as the ratio between a typical horizontal length $L$ and the liquid depth $d$: $\Gamma=L/d$). This forced pattern is very regular and can be characterized with a unique wavelength $\lambda_i$. When this wavelength is different from the optimal one, for the specific experimental condition, the pattern evolves to a final wavelength $\lambda_f$ inside the stability region. This evolution is generated by the dynamics of defects which yield a disorder in the pattern. In Sec. II a function which is used to describe quantitatively the disorder in the pattern is discussed and a two-dimensional model for convective pattern evolution is used. Section III is devoted to a brief description of experimental devices and of the thermal technique to force initial patterns. The main results of the evolution of wavelength, the disorder function and an evaluation of different contributions to the disorder, are, respectively, presented in Secs. IV and V. The discussion of these results and some conclusions are given in Sec. VI.

## II. DISORDER IN HEXAGONAL PATTERNS

A hexagonal pattern in Bénard convection ($B$) always shows some kind of defects which are different compared to those appearing in a pattern of rolls [2,9]. In that case the most frequent is the pentaheptagon pair which is associated to a dislocation line of the hexagonal pattern [10]. This two-dimensional (2D) hexagonal symmetry suggests dealing with some of the theoretical tools used to classify the disorder in 2D solids [2]. However, it must be stressed from the beginning that we work only by analogy, because the differences between Bénard cells and 2D solids are essential. The main one is that Bénard structure is of dynamical origin while structures in 2D are purely static.

In previous articles we analyzed the role of various parameters on the disorder of spontaneous patterns in $B$ convection [2]. Here a global parameter useful in classifying this disorder is briefly recalled: the disorder function $F_D$ defined as

$$F_D=\frac{1}{N}\sum_{j=1}^{N}\frac{1}{n_j}\sum_{i=1}^{n_j}\left|\ln\frac{l_{ij}}{\langle l\rangle}\right| , \tag{1}$$

where $n_j$ is the coordination number of the $j$th cell, $l_{ij}$ is the distance from the center of the $j$th cell to the center of its $i$th neighbor, $\langle l\rangle$ is the average of all the $l_{ij}$ but only the hexagons are considered, $N$ is the total number of cells. The cells in contact with the walls are not typical of the pattern because they are incomplete. So they are excluded in calculating $F_D$.

The disorder function $F_D$ is an average of the deviations of the distances between centers of the cells with respect to a simple regular pattern. It constitutes a global measure of the disorder and accounts for local defects as well as for orientational deviations or global bendings of hexagons in the pattern.

Other parameters have been introduced to classify the disorder in a hexagonal pattern. These are the percentage of defects and translational and orientational correlation functions [2]. However, these are useful only when the pattern has a considerable number of cells, in order to obtain good statistics. On the other hand, the disorder function $F_D$ gives significant results even in small aspect ratio vessels. In this situation the pattern can have no defects, but some orientational disorder is still present [2(b)]. For this reason, we have chosen this function to compare the disorder in vessels with a wide variety of aspect ratios and different shapes. $F_D$ is a good measurement of the disorder but it provides no information on its nature and its origin. To evaluate the various contributions to the dynamics, including defects, differences of the size of convective cells, the effect of lateral walls of the container, we use the so-called "amplitude equation" [11]. This describes quite well the fluid motion near the onset of convection. In this weakly nonlinear region the hydrodynamic variables can be written in the form

$$\mathbf{V}=\epsilon^{1/2}\left[\sum_{i=1}^{3}A_i e^{ik_c\mathbf{e}_i\cdot\mathbf{r}^*}\right]\mathbf{v}_0(z) , \tag{2}$$

where $\epsilon=(R-R_c)/R_c=(M-M_c)/M_c$ is the supercritical heating rate and $R$ and $M$ are the Rayleigh and the Marangoni numbers, respectively. The subscript $c$ denotes the critical values, $\mathbf{r}$ is a vector in the horizontal plane, and the asterisk superscript is the complex conjugate. The vector $\mathbf{v}$ is formed with the three components of the velocity field and the temperature deviations from the conducting profile. Here $k_c$ denotes the wave number at convective threshold, $\mathbf{e}_i$ stand for three unit vectors in the direction of the basic sets of rolls forming a hexagonal pattern, and $\mathbf{v}_0$ is a solution of the linear eigenvalue problem. When the three amplitudes $A_i$ take the same constant value and $\sum_i\mathbf{e}_i=0$, i.e., $\mathbf{e}_i\cdot\mathbf{e}_j=\cos(2\pi/3)$, Eq. (2) describes a perfect hexagonal pattern with a wave number $k_c$. The envelope functions $A_i$ that describe slow modulations of the pattern obey a set of equations

$$\tau_0\frac{\partial A_i}{\partial t}=\left[\epsilon+\xi_0^2\left[\frac{\partial}{\partial_{x_i}}-\frac{i\partial^2}{2\kappa_c\partial y_i^2}\right]^2\right]A_i - b_1 A_{i+1}^* A_{i+2}^* - \left[\sum_{j=1}^{3}b_j|A_j|^2\right]A_i \qquad (i=i \bmod 3) , \tag{3}$$

where the relaxation time $\tau_0$ and the correlation length $\xi_0$ can be obtained from a linear analysis. Coefficients $b_1$ and $b_{ij}$ stand for the coupling among different modes. They depend on the relative orientations $(\mathbf{e}_i\cdot\mathbf{e}_j)$ between pair of hexagonal lines. The derivatives $\partial/\partial x_i$ and $\partial/\partial y_i$ are the spatial derivatives parallel and perpendicular to vector $\mathbf{e}_i$, respectively. These equations allow us to account for spatial inhomogeneities in the pattern.

Equations (3) can be written in the form

$$\tau_0\frac{\partial A_i}{\partial t}=-\frac{\partial P}{\delta A_i^*} , \tag{4}$$

where $P$ is a potential defined as

$$\mathbf{P}=\int dx\,dy\left[\sum_{i=1}^{3}\left\{-\epsilon|A_i|^2+\left[\xi_0^2\left[\frac{\partial}{\partial x_i}-\frac{i\partial^2}{2\kappa_c\partial y_i^2}\right]A_i\right]^2\right\}+b_1\prod_{i=1}^{3}A_i^*+\tfrac{1}{2}\sum_{i=1}^{3}\sum_{j=3}^{3}b_{ij}|A_i|^2|A_j|^2\right] \tag{5}$$

provided that on the lateral boundaries $A_i=\partial A_i/\partial y_i=0$. The time derivative of this functional $P$ gives

$$\frac{dP}{dt}=-2\tau_0\int dx\,dy\sum_{i=1}^{3}\left|\frac{\partial A_i}{\partial t}\right|^2, \tag{6}$$

which is always negative. The existence of solutions in the nonlinear regime imposes that the quartic terms must be greater than the quadratic negative one in Eq. (5). The cubic one does not have a well-defined sign. However, nonlinear studies on $B$ convection [4(c)] and in situations where a hexagonal pattern develops itself (non-Boussinesq conditions, temperature modulation on the cell, etc.) [12] indicate that $b_1 \ll \sum_{i,j} b_{ij}$ [otherwise the development in Eq. (2) would not be valid]. As a consequence, one can assume that the cubic term in Eq. (5) gives only a small contribution to $P$. With these restrictions this functional is positive, while its temporal derivative is always negative: it is a Lyapunov functional. This ensures the asymptotic stability of the system.

Following the analysis of Cross [13], the functional $P$ can be split into three contributions, one from sidewall effects $P_S$, one from bulk effects $P_B$, and the third from defects $P_d$.

### A. Sidewall contributions

Close to the sidewalls, convective motions are constrained to take some preferred orientations. In the case of rolls, for example, these tend to go normal to the sidewalls. Recent works [13,14] showed that this effect can be explained in terms of the properties of Lyapunov potential. The amplitude of a convective roll approaching with an arbitrary angle to a plane sidewall takes the form

$$A=\left[\frac{\epsilon}{B}\right]^{0.5}\tanh\left[\frac{x}{\xi_0\cos\theta}\left[\frac{\epsilon}{2}\right]^{0.5}\right], \tag{7}$$

where $\theta$ is the angle between the roll normal and the wall normal (this solution is not valid for $\theta=0$ because in this case fourth-order derivatives must be taken into account [13]). This contributes to the Lyapunov functional as

$$P_S=\tfrac{1}{3}(2\epsilon)^{3/2}\xi_0\oint\cos\theta\,dl\ . \tag{8}$$

In the case of rolls perpendicular to lateral walls this contribution is of order $P_S\alpha\epsilon^{7/4}$, smaller than the contribution of oblique cells when $\epsilon\ll 1$ [13].

Hexagonal patterns form on the lateral walls polygonal cells with two sides perpendicular to the walls and with two sides at $2\pi/3$ rad with the walls [see Fig. 1(a)]. In the immediate vicinity of the wall only one mode perpendicular to the sidewalls prevails. At some distance, typically of the order of $\lambda/2$, three modes at $2\pi/3$ develop. Another possible orientation is represented in Fig. 1(b), where the three directions of the hexagonal lattice form $\pi/2$ and $\pm\pi/3$ with a sidewall, respectively. However, this configuration corresponds to a higher value of $P_S$, and therefore it is less stable than the previous one. This result could explain why the hexagonal cells in contact with a vessel wall are perpendicular to it in a steady regime. As we will see below, in transient regimes the nonperpendicular cells disappear very quickly.

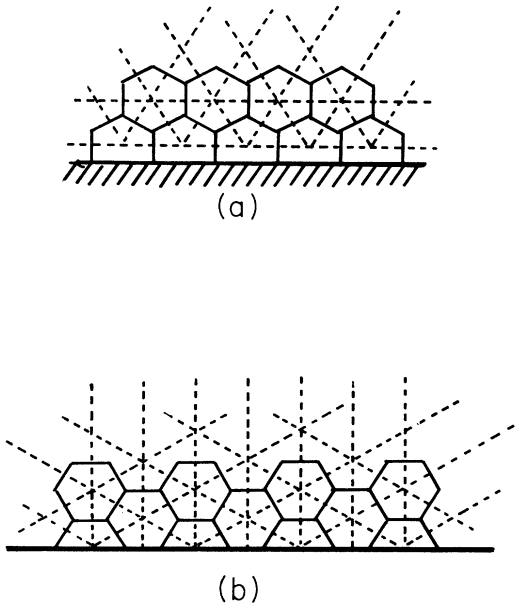


FIG. 1. Two possible orientations for the cells in contact with a vessel sidewall and the corresponding modes: (a) stable, (b) unstable.

### B. Bulk contributions

By analogy with a roll pattern it is proposed for the bulk contribution in the hexagonal case the following expression:

$$\mathbf{P}_B=\xi_0^2\epsilon\int dx\,dy\sum_{i=1}^{3}\left[\frac{1}{4k_c}\frac{\partial^2\Phi_i}{\partial y_i^2}+\left\{\left[\frac{\partial\Phi_i}{\partial x_i}\right]+\frac{1}{2k_c}\left[\frac{\partial\Phi_i}{\partial y_i}\right]^2\right\}\right], \tag{9}$$

which can be rewritten in a more suitable form

$$\mathbf{P}_B=\epsilon\xi_0^2\int dx\,dy\sum_{i=1}^{3}[(\mathrm{div}\mathbf{n}_i)^2+(\delta k_i)^2], \tag{10}$$

where the contribution of $b_1$ is neglected. Here the vectors $\mathbf{n}_i$ are defined as

$$\mathbf{n}_i=\left[0,\frac{1}{k_c}\frac{\partial\Phi_i}{\partial y_i}\right], \tag{11}$$

in coordinates $(x_i,y_i)$, and where $\delta k_i$ is the local variation of the wave number of the $i$th set of cell lines, that is,

$$\delta k_i=\frac{\partial\Phi_i}{\partial x_i}+\frac{1}{2k_c}\left[\frac{\partial\Phi_i}{\partial y_i}\right]^2 . \tag{12}$$

(Although small, the cubic term in $P$ imposes a link among the phases $\phi_1+\phi_2+\phi_3=0 \bmod 2\pi$.) As stressed by Heutmaker, Frenkel, and Gollub [15] this seems to be the most important contribution to the Lyapunov functional.

### C. Defect contributions

The most typical defect in hexagonal patterns is a pentagon-heptagon pair of cells. They correspond to simultaneous dislocations on two of the three systems of rolls forming the hexagonal pattern [16] (a typical situation in a Bénard pattern is shown in Fig. 2). These defects correspond to a solution of the type $A_{i+1}=A_{i+2}=0$, $A_i\neq 0$. Therefore, a local transition from hexagons to a roll takes place in a penta-hepta pair [16].

To calculate the contribution of the defects, we follow the analogy with the case of a pattern of rolls. As argued by Cross [13] and Heutmaker, Frenkel, and Gollub [15] a dislocation gives an approximate contribution $P_D \propto \epsilon^2$ (core area). Taking only into account penta-hepta pairs as the main defects in a hexagonal pattern, this contribution can be written in the form

$$P_d=\epsilon^2 N_d\,\pi r_c^2 , \tag{13}$$

where $r_c$ is the radius of the dislocation core, which can be estimated to be $\xi_0\epsilon^{-1/2}<r_c<2\xi_0\epsilon^{-1/2}$.

Although in these evaluations some rough simplifications have been made, they provide expressions that allow us to evaluate the evolution of patterns in a more quantitative manner.

## III. EXPERIMENTAL METHOD

The experiments are performed in a square box with a bottom made of copper and lateral walls made of perspex with a side length $L=25$ cm. In the present experiments several aspect ratios are used: $\Gamma_1=28.5$, $\Gamma_2=31.1$, $\Gamma_3=46.1$, $\Gamma_4=62.5$, and $\Gamma_5=65.3$, which correspond to $d=0.878$, 0.804, 0.542, 0.401, and 0.383 cm and they contain about 65, 87, 203, 401, and 440 complete cells, respectively. The heating device, the temperature regulation, and the method of determining the liquid depth

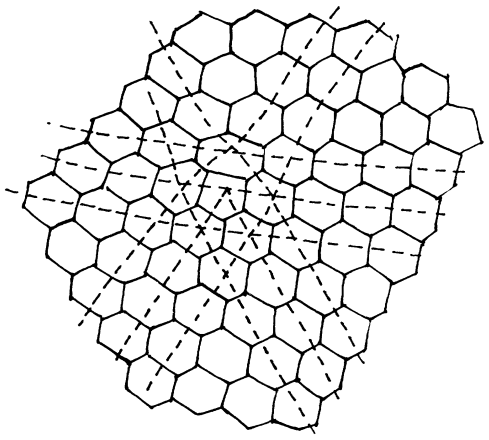

FIG. 2. A pentagon-heptagon pair in a convective hexagonal pattern (traced from a photograph).

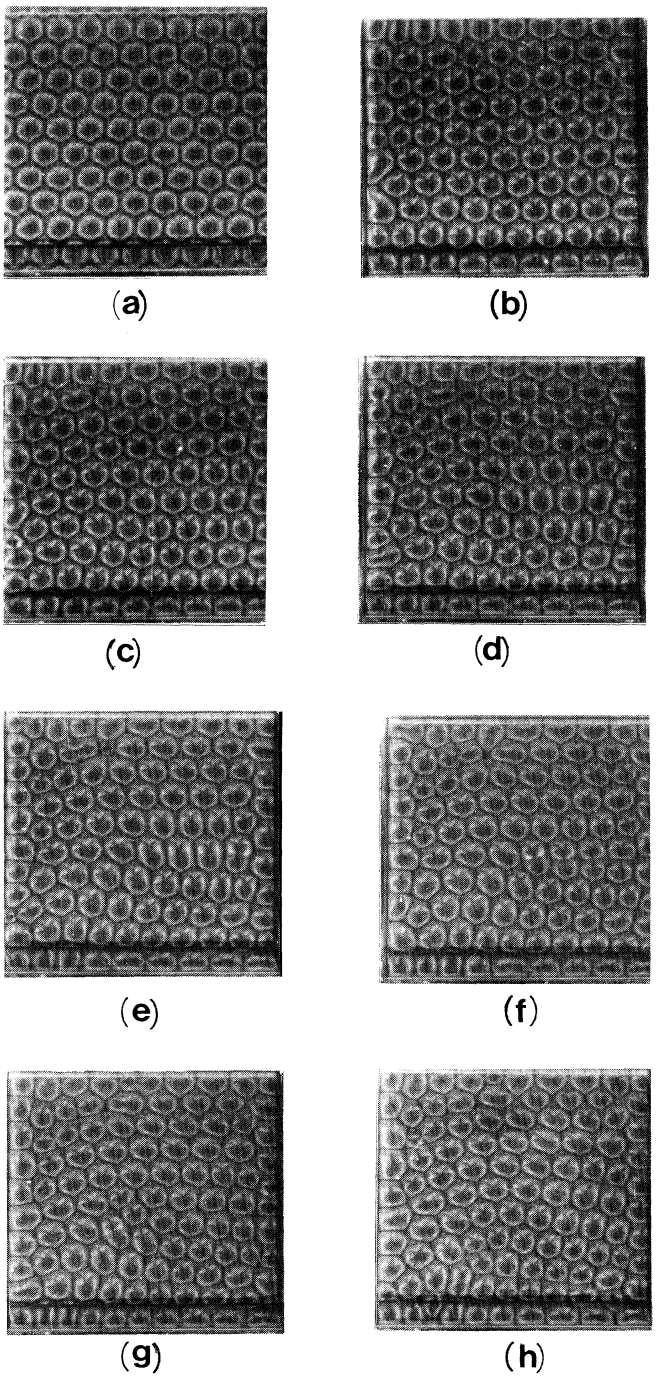


FIG. 3. Evolution of an imposed pattern in a small-aspect-ratio container. $\Gamma_1=28.5$, $\epsilon=2.2$. (a) $t=5$ s; (b) $t=1$ h 25 min; (c) $t=2$ h 7 min; (d) $t=2$ h 26 min; (e) $t=3$ h 50 min; (f) $t=4$ h 26 min; (g) $t=5$ h 30 min; (h) $t=6$ h 50 min.

have been described elsewhere [10]. The liquid used is silicon oil Rhodorsil 47V100, with a mean viscosity of 1 S and a Prandtl number Pr=880.

The motions in the fluid are visualized using either some aluminum powder or a shadowgraph technique [6] (the latter is based on the variation of the refractive index of the oil and on the deformation of the free surface with temperature). A lamp placed upon the convective vessel shines vertically down the pattern. The bottom of the container is polished to a mirror finish. The light reflected by this bottom plate is finally deviated by a beam splitter to a translucent screen. To follow its evolution, photographs of the pattern are taken at regular time intervals. These are digitized with a numerical procedure [2]. With suitable software the disorder function in each situation can be obtained.

Now, an experimental method to induce an initially perfect pattern is described in some detail. It has been used previously to induce a single hexagon in a box with a very small aspect ratio and to follow the stability of an imposed pattern of rolls [8]. This technique is based on the following fact. When a metallic tip touches the free surface, this point becomes a cold point because heat flows easily up across the metal. As a consequence, the corners of three hexagons (i.e., a cold point of the pattern) are formed in the contact point. Therefore a regular arrangement of metallic rods, set through a plate with the chosen regularity, is built. Then the plate with the rods is set upon the free surface and lowered until the rod tips just touch the surface. With rods in contact, the fluid is heated until convective cells appear. When convection is well developed the plate with the rods is removed and a very regular pattern can be viewed [Fig. 3(a)].

## IV. EVOLUTION OF IMPOSED PATTERNS

The measurements have been performed in vessels with different aspect ratios set in an interval from 28.5 to 65.3. For smaller vessels ($\Gamma < 20$) systematic measurements are not available because the number of cells is too small, the influence of the lateral walls very important, and the pattern becomes quite irregular quickly. On the other hand, it has been demonstrated in a previous work [17] that, when $\Gamma > 70$, the liquid layer can be considered as infinite. The distance to the threshold $\epsilon$ has been fixed to values ranging from 0.6 to 2.2.

For a fixed pattern, results are gathered for (i) small aspect ratios ($\Gamma_1=28.5$ and $\Gamma_2=31.3$), (ii) intermediate ($\Gamma_3=46.1$), and (iii) large ($\Gamma_3=62.5$ and $\Gamma_4=65.3$) aspect ratio vessels. In each of these vessels regular hexagonal patterns with $k$ smaller or larger than the optimal one (for the experimental conditions) are forced initially and their time evolution is followed. The optimal wavelength corresponds to an average wavelength of the final pattern (in fact, one notices that this average slightly fluctuates after several hours). These optimal values are in agreement with those obtained in spontaneous patterns for similar situations [17,18].

The kinetics of the evolution depends on various parameters $\lambda_i$ (the initial wavelength), $\Gamma$, $\epsilon$, and the size of

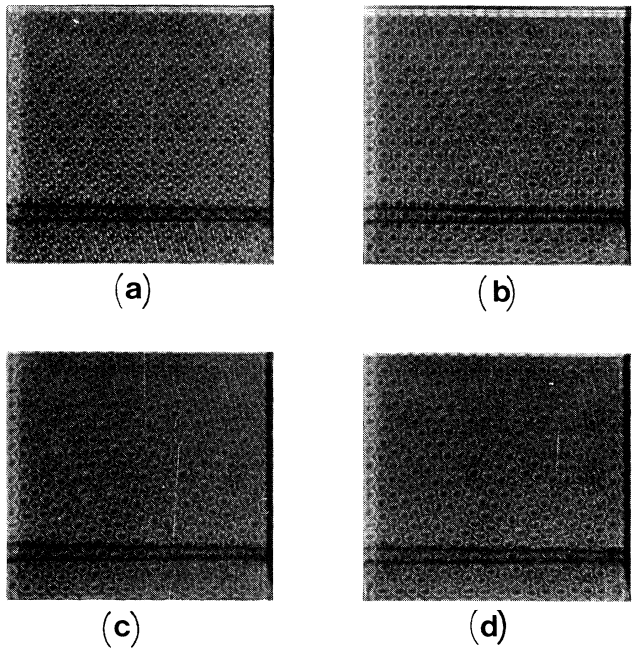


FIG. 4. Evolution of an imposed pattern in a large-aspect-ratio container. $\Gamma_5=65.3$, $\epsilon=0.6$. (a) $t=10$ s; (b) $t=24$ min; (c) $t=2$ h 48 min; (d) $t=3$ h 12 min.

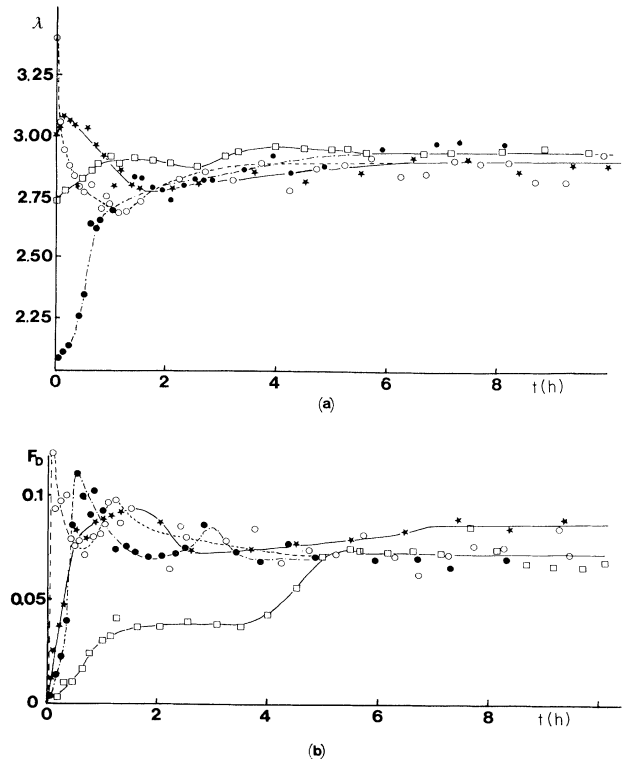


FIG. 5. Evolution of a perfect imposed pattern as a function of time $\epsilon=2.2$. (a) Mean wavelength, (b) disorder function. $\Gamma_1=28.5$; $\lambda_i=0.94\lambda_f$, □; $\lambda_i=0.72\lambda_f$, ●; $\lambda_i=1.17\lambda_f$, ○. $\Gamma_2=31.1$: $\lambda_i=1.003\lambda_f$, ★.

cells in contact with the sidewalls. When the pattern evolves spontaneously, the appearance of the structural disorder, the breakup of a cell or the "fusion" of two cells, or the disappearance of a cell are observed anywhere in the vessel, whereas the mean size of the other cells varies until they reach the optimal value.

The results are gathered in two subsections. In the first we quote the evolution of the average wavelength $\lambda$ and the disorder function $F_D$. The second deals with a more specific question: the influence of the lateral walls in this evolution.

### A. Evolution of $\lambda$ and $F_D$

Two examples of the dynamics of forced patterns can be seen in sequences of photographs in Figs. 3 and 4. From Figs. 3(a) and 4(a) it is obvious that the thermal technique provides perfect initial patterns. (The sequences will be examined in more detail in the following subsection). The main experimental results are summarized in Fig. 5 for small aspect ratio vessels and in Fig. 7 for intermediate and large aspect ratios. We comment on these results separately.

#### 1. *Small aspect ratios* ($\Gamma_1=28.5$, $\Gamma_2=31.1$)

The evolution of the mean wavelength $\lambda$ appears in Fig. 5(a). The heating rate is fixed at $\epsilon=2.2$. Different

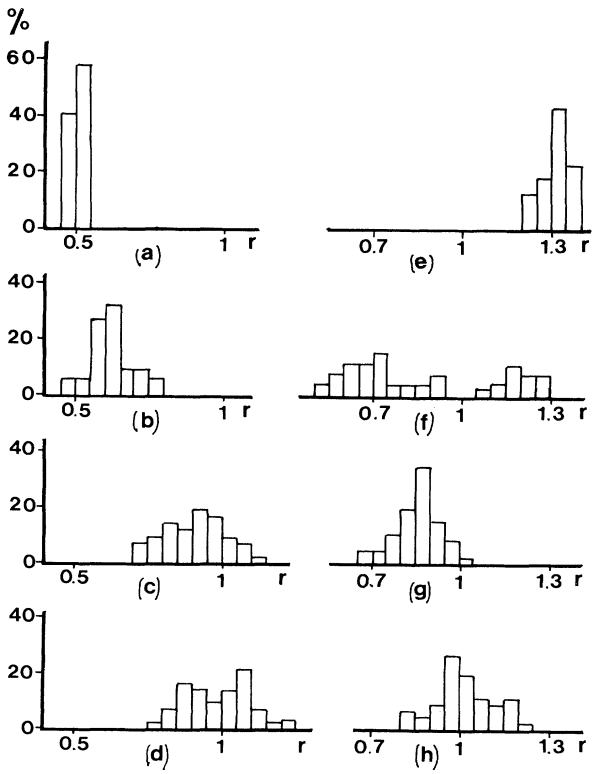


FIG. 6. Histograms of $r=(\lambda/\lambda_f)^2$ for $\Gamma=28.5$ and $\epsilon=2.2$. $\lambda_i=0.72\lambda_f$: (a) $t=0$; (b) $t=32$ min; (c) $t=2$ h 6 min; (d) $t=3$ h 53 min. $\lambda_i=1.17\lambda_f$: (e) $t=10$ s; (f) $t=5$ min; (g) $t=1$ h 32 min; (h) $t=7$ h 14 min.

initial $\lambda$ have been imposed, but it is clear that the final wavelength is the same, whatever the initial wavelength. In this case the final wavelength is about 2.9. This value shows fluctuations because the pattern is not completely stationary. The amplitude of these fluctuations decreases when $\Gamma$ increases, showing the influence of the walls on the structure. In most cases, the time necessary to reach this final value is about 5 h, much greater than that for larger containers.

It is interesting to notice that the evolution of the pattern depends on the sign of $\delta\lambda=(\lambda_i-\lambda_f)/\lambda_f$ (here $\lambda_i$ indicates the initial wavelength and $\lambda_f$ is the final mean wavelength). When $\delta\lambda$ is positive, $\lambda$ reaches a minimum and increases later on. This can be interpreted in the following manner. The large hexagons tend to break and to nucleate smaller ones. In the first steps of this evolution many large hexagons break rather quickly (1 or 2 h). Then the competition among small hexagons tending to grow leads to a global increase of $\lambda$.

On the contrary, when $\delta\lambda<0$, $\lambda$ evolves monotonously and a maximum is not reached before the final value. That means that when the forced hexagons are too small, some of them push on some of their neighbors and a fusion of two hexagons is observed (no regularity has been detected in this fusion progress). As a result $\lambda$ increases, reaching its mean final value $\lambda_f$ after 5 h.

As a general feature, the evolution of hexagons when $\delta\lambda<0$ is faster in the first steps (about 1 h). Afterwards, the pattern rearranges itself more slowly. It is interesting to compare this behavior with the evolution of the disorder function $F_D$ in Fig. 5(b) and the histogram of $r=(\lambda/\lambda_f)^2$ in Fig. 6. At $t=0$, taking into account the experimental uncertainties there is only one wavelength $\lambda_i$, so $F_D=0$. But this situation is unstable (it will be discussed below). In particular when $\delta\lambda$ is large, and a few seconds after spontaneous evolution starts, the size of several cells has already slightly decreased [Fig. 6(e)], and the histogram has widened. Whatever the sign of $\delta\lambda$, the disorder function shows a sharp peak several minutes after the pattern is evolving freely. This means that a wide range of local wavelengths is present in the pattern. For instance, in Fig. 6(f) a great dispersion of $\lambda$ can be seen and two regions can be considered. The first one, from $r=0.5$ to 0.95 corresponds to small cells which appear from the breakup of large hexagons. These cells are mostly smaller than the final cells. The second region, from $r=1.1$ to 1.3, is due to the remaining initial cells which have suffered a small contraction. This situation is unstable so the pattern still evolves (first by fusion or nucleation of cells and afterwards by slower evolution of defects). The first process is a bulk process and seems not to be dependent on the aspect ratio. In the second, the side walls play an important role.

The disorder function shows a second maximum when $\Gamma$ is small (the physical interpretation of this fact from the photographs is not evident). Finally, $F_D$ attains a value which corresponds to the intrinsic disorder of the pattern for given $\epsilon$, $\Gamma$, and vessel geometry. This final value decreases when $\Gamma$ increases. Strong fluctuations around this value can be observed when $\Gamma$ decreases. Small fluctuations of $\lambda_f$ are also observed. Histograms

6(d) and 6(h) show that the allowed wavelengths occur in a bandwidth which is about $0.1\lambda_f$.

### 2. *Intermediate and large aspect ratios ($\Gamma_3=46.1$, $\Gamma_4=62.5$, $\Gamma_5=65.3$)*

In this case the heating rate is taken constant at $\epsilon=0.6$. The main results are summarized in Fig. 7. Forced patterns evolve to $\lambda_f=2.9$, almost the same as in small aspect ratio vessels. For $\Gamma_3$ and $\delta\lambda>0$ a minimum is still evident, but not for larger $\Gamma$. As observed in the preceding subsection, the evolution for comparable $\delta\lambda$ and the same $\Gamma$ is faster when $\delta\lambda>0$ than in the contrary case. The final value is reached 3 h after the free evolution of the initial pattern.

The disorder function in the intermediate case ($\Gamma=46.1$) behaves in a similar manner to the small $\Gamma$ case. It shows a sharp maximum at initial stages, followed by a valley, and afterwards a slow increase. This behavior is due to the sudden elimination ($\delta\lambda<0$) or nucleation ($\delta\lambda>0$) of many cells in the initial pattern. Later on, the pattern rearranges itself and the disorder function reaches a saturation value. When $\Gamma$ is large, the behavior is more uniform, and the saturation value for $F_D$ and the corresponding fluctuations, smaller than in the preceding case, are obtained, in accordance with previous results [17].

Finally it can be noticed that in all cases $\lambda_f$ is reached before or at the same time as the final value of $F_D$, never after. This means that the optimal size of the system is obtained while structural rearrangements are still occurring.

### 3. *Time evolution of the pattern*

During the first steps of the pattern variation, the evolution of the disorder can be characterized by the distortion velocity defined by $V_D=dF_D/dt^*$, where $t^*$ is written in nondimensional form with a time scale $(\rho d^3/\sigma'\Delta T)^{0.5}$; $\rho$ is the density, $d$ is the depth layer, $\sigma'$ is the temperature coefficient of surface tension, and $\Delta T$ is the temperature difference between the lower and the upper surfaces.

It is clear in Fig. 8 that $V_D$ increases when $|\delta\lambda|$ increases. It must be noticed that $V_D$ is small, but different from zero when $\delta\lambda=0$, because the imposed wavelength is not the only phenomenon destabilizing the structure. Indeed, the intrinsic disorder and the sidewalls (this is mentioned in the next paragraph) force the pattern to distort even if $\lambda_i=\lambda_f$.

## B. Some effects on the lateral walls

We analyze in more detail some interesting features observed when the forced pattern has a slightly smaller $\lambda_i$ than the optimal one ($\delta\lambda<0$). When $\Gamma=28.5$ the evolution is shown in the series of photos in Fig. 3. The initial pattern has $\lambda_i=2.73$. It is formed by 17 columns of complete hexagons and two columns of half hexagons, and 10 rows of complete hexagons and two rows of fractional hexagons. It is a general observation that for $B$ experiments in a permanent regime the cells attached to the lateral walls are perpendicular to them (this feature has also been noticed in roll patterns) [14]. In photo 3(b) it can be seen that the cells near the walls tend to get normal to them to satisfy this general rule. To fulfill this requirement the small cells (in fact, portions of cells) initially in contact with the walls are "absorbed" by their neighbors which finally attach themselves perpendicular-

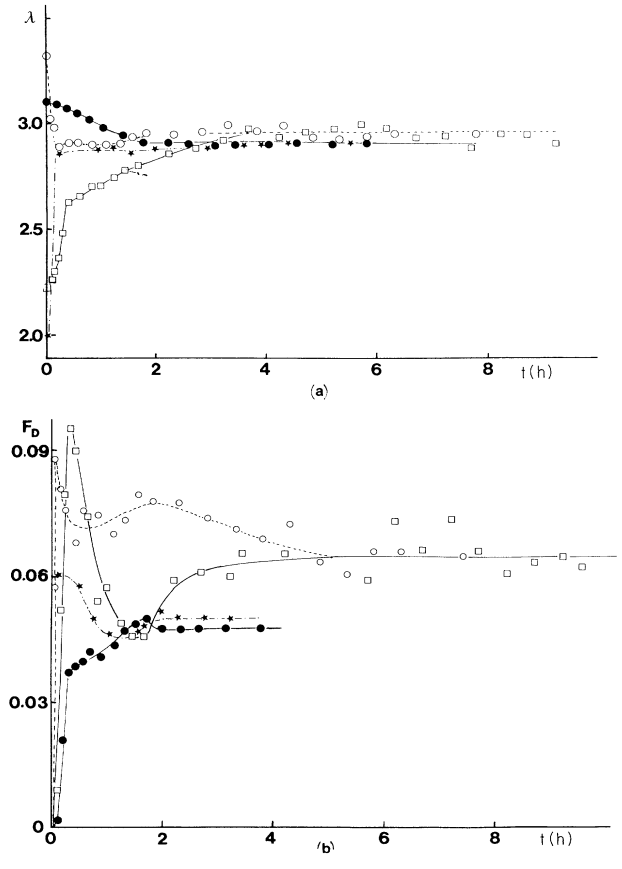


FIG. 7. Evolution of a perfect imposed pattern as a function of time. (a) Mean wavelength, (b) disorder function. $\Gamma_3=46.1$: $\lambda_i=0.77\lambda_f$, □; $\lambda_i=1.14\lambda_f$, ○; $\Gamma_4=62.5$: $\lambda_i=0.69\lambda_f$, ★; $\Gamma_5=65.3$: $\lambda_i=1.07\lambda_f$, ●.

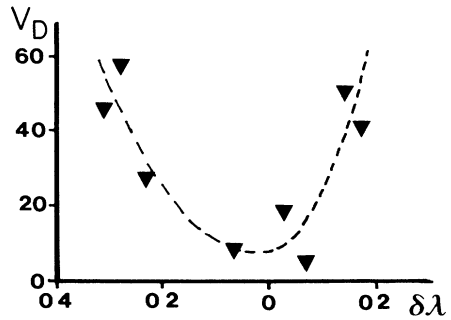


FIG. 8. Pattern disorder veocity as a function of $\delta\lambda=(\lambda_i-\lambda_f)/\lambda_f$.

ly to the sidewalls. The disappearance of these portions of cells elongates the pattern in the same direction, creating some kinds of "stress." But the situation is different for the two directions fixed by the walls. On "vertical" sidewalls there are half hexagons and complete hexagons in oblique contact, whereas on "horizontal" sidewalls only fractions of cells (less than half a hexagon) are attached perpendicularly to them. In Fig. 3(b) it can be seen that on "vertical" sidewalls the hexagons tend to reorientate themselves to get normal to those walls, creating an orientational disorder. But most important are the effects on the horizontal sidewalls because the initial rows of fractional cells are "absorbed" by their neighbors, which become perpendicular to those walls, creating some vertical stresses. These stresses and the existence of a wavelength selection mechanism modify the shape and the size of all cells in the whole pattern.

In this particular case, the breaking of cells is so well organized that it corresponds to the propagation of a dislocation. It is observed in the subsequent evolution of the pattern in Figs. 3(c)–3(h). The most remarkable fact is the evolution of a single dislocation that appears in the sixth row from the top right. First, the rows 5 and 6 are distorted in the vertical direction as a consequence of the stresses. Then, in spite of the orientational disorder induced by the vertical sidewalls (which is visible mainly at the top left), more important wavelength selection mechanisms exist. On one hand, there is a rearrangement on the horizontal sidewalls (inducing an increase in the mean wavelength) and, on the other hand, there are the stresses provoked by this effect. These facts lead to the creation of a dislocation line that climbs from the right to the left decreasing the mean wavelength. Its evolution is shown in Fig. 9(a). It is noteworthy that the curve is very similar to the behavior of strain versus time in a viscoelastic medium when a constant stress is applied.

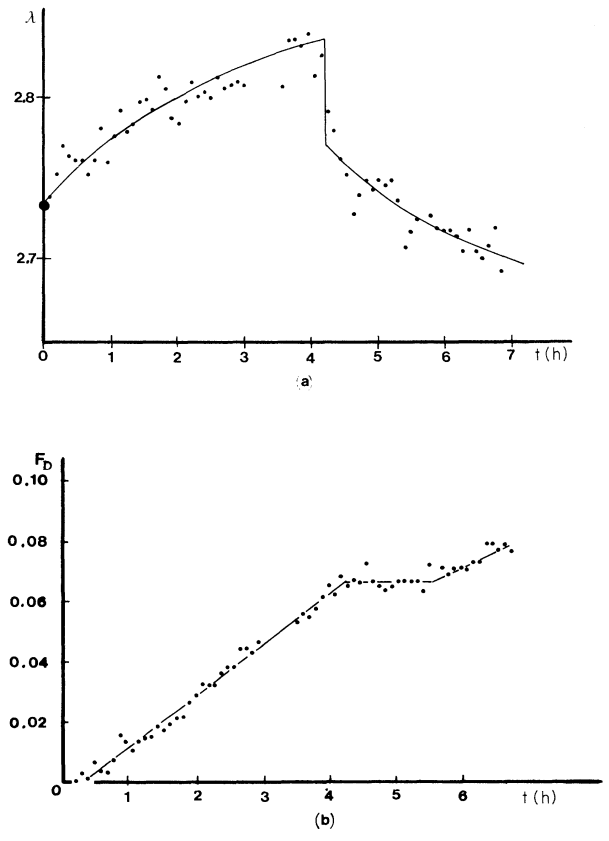


FIG. 9. Evolution of a perfect imposed pattern in a small-aspect-ratio container ($\Gamma_1=28.5$): (a) mean wavelength, (b) disorder function.

The evolution of the disorder function $F_D$ is shown in Fig. 9(b). It can be concluded that, to begin with, the number of defects (pentagons and heptagons) increases to satisfy the boundary conditions. During the climbing of the dislocation, $d_D$ diminishes. Afterwards, it increases again, until it reaches a saturation value similar to that observed in a previous experiment [19]. The disorder function $F_D$ also increases, more or less linearly with time, showing a change in the slope at about 4.3 h, approximately when the dislocation starts to climb.

The second case corresponds to $\Gamma=65.3$ and $\epsilon=0.6$. The initial wavelength is larger than the final one. The photos of Fig. 4 show the evolution in time in this case. It can be seen that the cells near the walls evolve as in the preceding case, also creating a stress. As a consequence of this stress, and as the imposed wavelength is too large, many cells in the center of the vessel become deformed [see Figs. 4(b) and 4(c)]. However, near the walls, domains with the initial regularity still remain. Afterwards, those elongated cells break up into smaller cells, leading to a rapid decrease in the mean wavelength, as will be seen below. No regularity in this splitting process has been observed.

## V. TRANSIENT PATTERN EVOLUTION AND THE LYAPUNOV FUNCTIONAL

We describe the behavior of the Lyapunov functional in the case corresponding to the evolution sequence of Fig. 5 (points). For a precise calculation of various contributions of $P$ we need further theoretical work to specify the values of $r_c$, $\xi$, and $B$. In this paper we want only to evaluate the relative importance of the four contributions $P_d$, $P_s$, $P_{B'}$, and $P_{B''}$ (which are the parts of $P_B$ corresponding, respectively, to the wave-number difference and to the wave-number divergence). For that reason we assume that $r_c$ and $\xi$ are close to that in Rayleigh-Bénard convection. We take $r_c=1.5r_c\xi$ with $\xi=\xi_0\epsilon^{-0.5}$ and $\xi_0=0.4d$. For the reference wave number we use the experimentally measured wave number selected in the final structure. Figure 10 shows the results of our experimental measurement of the four parts of $P$ (the lengths are measured in units of the depth layer). For the first steps of the experiment, $P_{B''}$ and $P_d$ are zero. The model shows that the disorder appears because of the size effect of the imposed cells and of the orientation of the cells in contact with the walls. For this experiment $P_s$ is greater than $B_{B'}$: the wall effect is the most important when experi-

ment starts. Then the cells quickly become perpendicular to the walls: $P_s$ decreases and becomes almost zero. In the same time the sizes of the cells decrease and, as a consequence, the lines joining the centers of the cells are progressively curved and the number of defects increases. That perturbations of the pattern induce a new disorientation of the cells in contact with the walls: $P_s$ increases and goes through a maximum which corresponds to the maximum of mean wavelength [Fig. 5(a)] and to large variations of $F_D$ [Fig. 5(b)]. After 3 h, $P_s$, $P_{B'}$, and $P_{B''}$ decrease whereas $P_d$ is nearly constant.

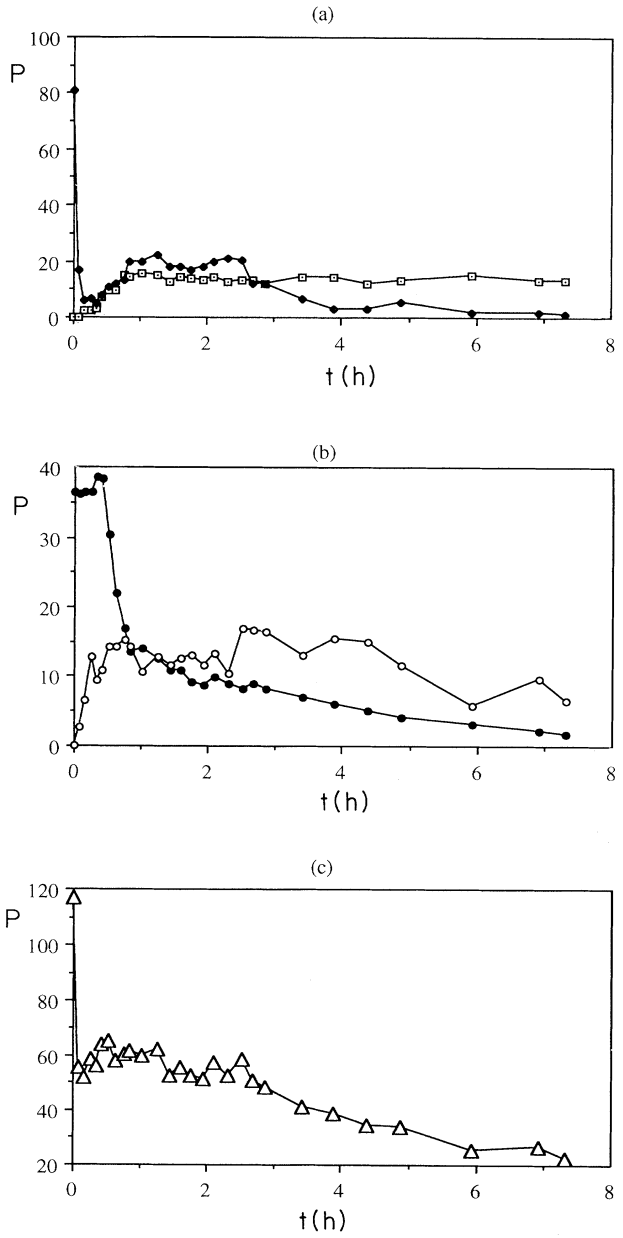


FIG. 10. Lyapunov functional contributions vs time. (a) Defects $P_d$, □; sidewall $P_s$, ◆. (b) Wave number $P_{B'}$, ●; wavevector divergence $P_{B''}$, ○. (c) Total Lyapunov functional $P$, △.

## VI. DISCUSSION AND CONCLUSION

It has been proved that the thermal technique provides an efficient tool to force a hexagonal pattern in $B$ convection. This is applied to study the evolution of forced patterns. This evolution depends on the relative difference $\delta\lambda$ between the imposed $\lambda_i$ and the optimal $\lambda_f$, on the aspect ratio, on the heating rate $\epsilon$, and on the vessel shape.

In the present work, the influence of $\delta\lambda$ and of $\Gamma$ on hexagonal patterns in square vessels at fixed $\Gamma$ have been analyzed. When $\delta\lambda$ is sufficiently large, two mechanisms can appear. These are nucleations of small hexagons (when $\delta\lambda > 0$) or fusion of small hexagons to form larger ones (when $\delta\lambda < 0$). This leads to a variation in $\lambda$ that, in most cases, is far from monotonous. These mechanisms appear in the bulk (mainly in the center) of the pattern. In small vessels the sudden nucleation of many cells leads to a minimum in the mean $\lambda$, which increases later on. However, for fusion effects, $\lambda$ increase monotonously.

The disorder function shows a sudden increase when the pattern evolves freely from a forced pattern, later reaching a saturation value, which manifests that a finite bandwidth of local wavelengths is present in the pattern [21]. As expected, the effects of lateral walls decrease when $\Gamma$ increases. An interesting result has been obtained in small vessels when $\delta\lambda > 0$. In this case boundary effects force the pattern to rearrange itself in an unexpected manner: the system tends to reach the optimal wavelength by generation of a dislocation line. Although more detailed experiments are desirable, one can conclude that the dislocation mechanism also provides a wavelength selection mechanism in hexagonal patterns.

It has been proved theoretically by Siggia and Zippelius [20], Pomeau, Manneville, and Zaleski [21], and experimentally by Croquette and Pocheau [22], that the climb of a dislocation line provides a good wavelength selection mechanism in a pattern of rolls in RB convection. We now have some evidence that, for a small aspect ratio, this can also be the case for a hexagonal pattern.

An important difference exists between the experimental results of Croquette and Pocheau [22] and of Whitehead [23] and the present ones: in the first two cases, the dislocation was initially imposed whereas in this hexagonal case the formation and evolution of such a dislocation are spontaneous. The lateral tensions, a consequence of the boundary conditions, lead to a broadening of some row in one direction, which leads finally to the division of some cells forming a dislocation line, which has not been observed before in surface-driven Bénard convection to our knowledge. In fact, that this behavior is different from it could be inferred considering hexagons simply as the superposition of three rolls, where it can be expected that some kind of zigzag instability would appear. Here, the system seems to prefer this dislocation mechanism to turn up to the stability region. These features, however, suggest some questions about the universality of this mechanism, on its dependence on the aspect ratio, and also on the influence of the nonlinear coupling between oblique modes, specific to this hexagonal case, and finally on possible secondary instabilities. Numerical simulations such as that made by Bestehorn and Haken [24], following the lines of the work of Siggia and Zippelius

[20], could clarify this point.

The amplitude equation for a hexagonal pattern allows us to estimate the relative importance of various contributions to disorder: structural defects, curvature of the cell rows, wave-number variations, and wall effects. It would be desirable to test this model for other experimental cases such as range of $\epsilon$, vessels with special shapes, nonvariational effects, etc.


[1] *Cellular Structures in Instabilities,* edited by J. F. Weisfreid and S. Zaleski, Lecture Notes in Physics Vol. 210 (Springer, Berlin, 1984).

[2] (a) R. Occelli, E. Guazzelli, and J. Pantaloni, J. Phys. Lett. **4**, L597 (1983); (b) P. Cerisier, R. Occelli, C. Pérez-Garcia, and C. Jamond, J. Phys. **48**, 569 (1987).

[3] H. Bénard, Rev. Gén. Sci. Pur. Apl. **11**, 1261 (1900).

[4] (a) O. W. Scanlon and L. A. Segel, J. Fluid Mech. **30**, 149 (1967); (b) S. Rosenblat, S. H. Davis, and G. H. Homsy, *ibid.* **120**, 91 (1982); **120**, 123 (1982); (c) A. Cloot and G. Lebon, *ibid.* **145**, 447 (1984).

[5] For a review see F. H. Busse, Rep. Prog. Phys. **41**, 1929 (1978).

[6] N. M. Chen and J. A. Whitehead, J. Fluid Mech. **38**, 279 (1969).

[7] F. H. Busse and J. A. Whitehead, J. Fluid Mech. **47**, 305 (1971); **66**, 67 (1974).

[8] P. Cerisier, C. Pérez-Garcia, C. Jamond, and J. Pantaloni, Phys. Lett. **112A**, 366 (1985); P. Cerisier, C. Pérez-Garcia, C. Jamond, and J. Pantaloni, Phys. Fluids **30**, 954 (1987); P. Cerisier, J. Pantaloni, and C. Pérez-Garcia, Phys. Chem. Hydrodyn. **10**, 341 (1988).

[9] P. Cerisier and J. Pantaloni, in *Cellular Structures in Instabilities* (Ref. [1]), p. 197.

[10] P. Cerisier, J. Pantaloni, G. Finiels, and R. Amalric, J. Appl. Opt. **21**, 2153 (1982).

[11] A. C. Newel and J. A. Whitehead, J. Fluid Mech. **38**, 279 (1969); L. A. Segel, *ibid.* **38**, 203 (1969); G. Ahlers, M. C. Cross, P. C. Hohenberg, and S. Safran, *ibid.* **110**, 297 (1981).

[12] E. Palm, J. Fluid Mech. **8**, 183 (1960); F. H. Busse, *ibid.* **30**, 625 (1967); M. N. Roppo, S. H. Davis, and S. Rosenblatt, Phys. Fluids **27**, 796 (1984).

[13] M. C. Cross, Phys. Rev. A **25**, 1065 (1982).

[14] S. Zaleski, Y. Pomeau, and A. Pumir, Phys. Rev. A **29**, 366 (1984).

[15] M. S. Heutmaker, P. N. Frenkel, and J. P. Gollub, Phys. Rev. Lett. **54**, 1369 (1985).

[16] S. Ciliberto, P. Coullet, J. Lega, E. Pampaloni, and C. Pérez-Garcia, Phys. Rev. Lett. **65**, 2370 (1990).

[17] P. Cerisier, C. Pérez-Garcia, C. Jamond, and J. Pantaloni, Phys. Rev. A **35**, 4 (1987).

[18] P. Bergé and M. Dubois, in *Dynamical Critical Phenomena,* edited by C. P. Enz, Lecture Notes in Physics Vol. 104 (Springer, Berlin, 1979).

[19] Similar but more precise results in RB convection have been obtained by M. S. Heutmaker and J. P. Gollub, Phys. Rev. A **35**, 242 (1987).

[20] E. Siggia and A. Zippelius, Phys. Rev. Lett. **47**, 635 (1981); Phys. Rev. A **24**, 1036 (1981).

[21] Y. Pomeau, P. Manneville, and S. Zaleski, Phys. Rev. A **27**, 2710 (1981).

[22] V. Croquette and A. Pocheau, *Cellular Structures in Instabilities* (Ref. [1]), p. 104; A. Pocheau and V. Croquette, J. Phys. **45**, 35 (1984).

[23] J. A. Whitehead, J. Fluid Mech. **75**, 715 (1976).

[24] M. Bestehorn and H. Haken, Z. Phys. B **57**, 329 (1984); M. Bestehorn and C. Pérez-Garcia, Europhys. Lett. **4**, 12 (1987).

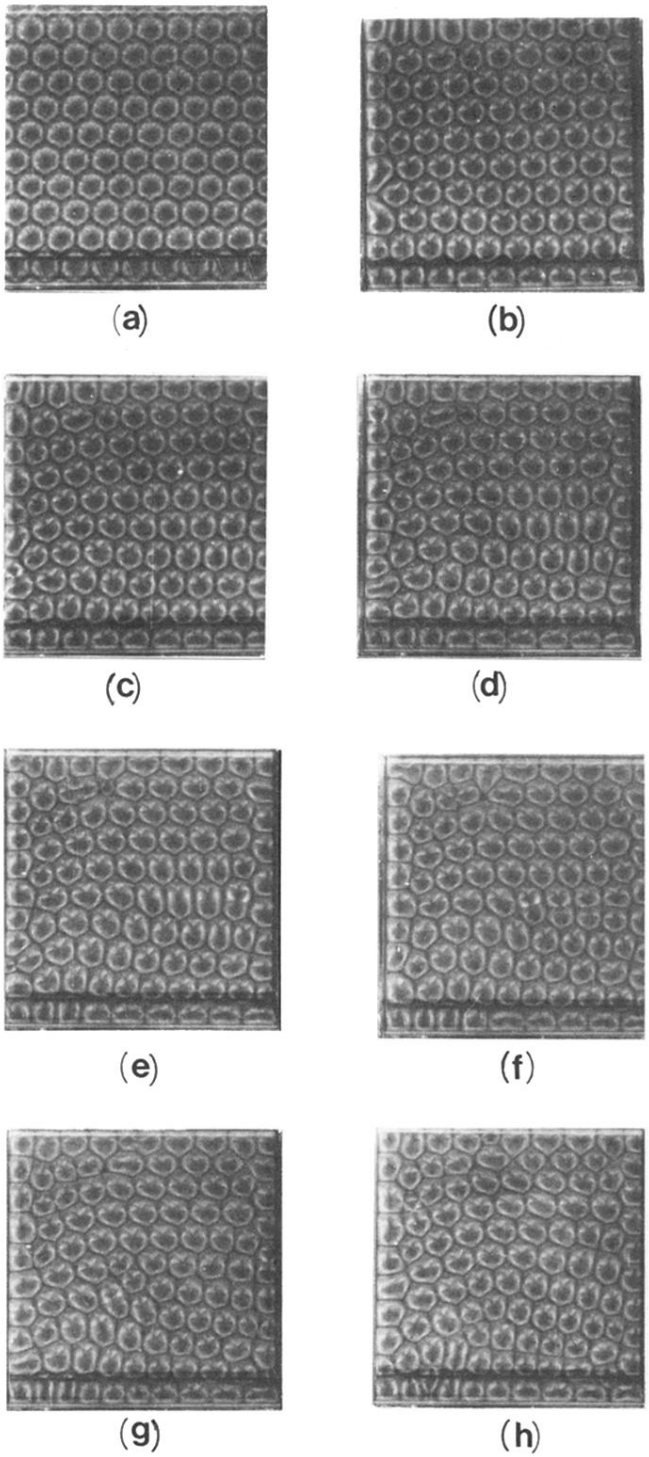


FIG. 3. Evolution of an imposed pattern in a small-aspect-ratio container. $\Gamma_1 = 28.5$, $\epsilon = 2.2$. (a) $t = 5$ s; (b) $t = 1$ h 25 min; (c) $t = 2$ h 7 min; (d) $t = 2$ h 26 min; (e) $t = 3$ h 50 min; (f) $t = 4$ h 26 min; (g) $t = 5$ h 30 min; (h) $t = 6$ h 50 min.

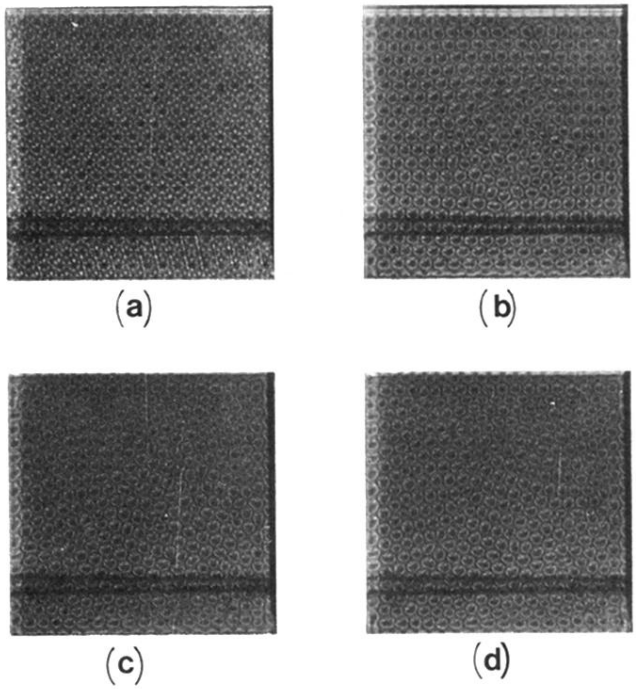


FIG. 4. Evolution of an imposed pattern in a large-aspect-ratio container. $\Gamma_5=65.3$, $\epsilon=0.6$. (a) $t=10$ s; (b) $t=24$ min; (c) $t=2$ h 48 min; (d) $t=3$ h 12 min.